ACS APPLIED BIO MATERIALS

www.acsabm.org Article

Development of a Label-Free LSPR-Apta Sensor for *Staphylococcus aureus* Detection

Heba Khateb, Gunnar Klös, Rikke L. Meyer, and Duncan S. Sutherland*

Cite This: https://dx.doi.org/10.1021/acsabm.0c00110 Read Online

ACCESS | Metrics & More | Article Recommendations | Supporting Information

ABSTRACT: The risk of foodborne diseases has increased over the last years. We have developed a simple, portable, and label-free optical sensor via aptamer recognition of *Staphylococcus aureus* at nanostructured plasmonic elements. The developed aptamers conjugated to a localized surface plasmon resonance (LSPR) sensing device were applied in both pure culture and artificially contaminated milk samples enabling a limit of detection of 10^3 CFU/mL for *S. aureus* in milk. There was no need for a pre-enrichment step, and the total analysis time decreased from 30 min to 120 s. Finite-difference time-domain was used to simulate the experimentally measured optical responses for a range of different sensor designs (100 and 200 nm disks), addressing the role of the near field and intrinsic refractive index sensitivity. A comparison of the aptamer to antibody-based recognition approaches showed that the thickness of the sensing layer was critical with a significantly larger response for the thinner aptamer layer. Comparison of differently sized metal nanostructures showed a significantly higher sensitivity for 200 nm diameter compared to 100 nm diameter disk structures resulting from both increases in bulk refractive index sensitivity and the extent to which the local field extends out from the metal surface. These findings confirmed that the developed gold nanodisk-based LSPR sensing chips could facilitate sensitive detection of *S. aureus* in food samples.

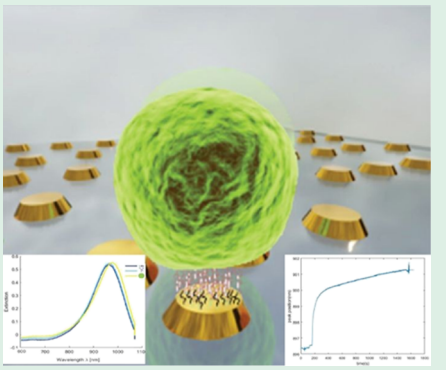

KEYWORDS: *LSPR apta-sensor, plasmonic biosensor, Staphylococcus aureus, detection, optical biosensors, CCP evaluation, food monitoring*

INTRODUCTION

Foodborne bacterial diseases have increased over the last few years[1−3] caused mainly by the pathogens *Salmonella typhimurium*, *Staphylococcus aureus*, *Listeria monocytogenes*, and *Escherichia coli*,[2] resulting in many deaths.[4,5] *S. aureus* is a Gram-positive, widespread, and highly virulent pathogen. Around 70% of strains are considered enterotoxigenic;[6] thus the potential for food poisoning still exists even with pasteurization, as the enterotoxin is heat resistant.[3,7] *S. aureus* has been found in various minimally processed foods and ready to eat foods[8−11] Further complications in treatment arise as antibiotic-resistant strains, such as methicillin-resistant *S. aureus*, have become more prevalent. Detection and diagnosis of pathogens in the food, in the environment, and at the point of care have been areas of strong technological development. However, conventional culture methods remain the most widespread technique for foodborne pathogen detection despite the slow response (days). Developments to improve sensitivity, rapidity, suitability, and specificity have been underway leading to methods including both optical and electrochemical approaches, for example, enzyme-linked immunosorbent assay[12] and real-time polymerase chain reaction (PCR),[13] electrochemical sensors,[14] impedimetric immunosensor,[15] and surface plasmon resonance sensors.[16] A trend in detection and measurement approaches has been toward label-free and rapid assays. Localized surface plasmon-based sensors are one promising approach that can provide compact and ultrasensitive measurements based on refractive index changes during recognition events.

Localized surface plasmon resonance (LSPR) has shown high performance for the detection of small biomolecules,[17] protein−protein interactions,[18] surface binding events, and pathogen detection[4,19−21] because of their high reproducibility, sensitivity, and label-free detection in real time.[22−26] Nagatsuka et al. have demonstrated LSPR detection systems for biological toxins that utilize glyco-chips with sensitivity down to 10−30 ng/mL.[23] Label-free LSPR for DNA detection was successfully demonstrated with an achievable limit of detection (LOD) of 5 nM with 2 h hybridization of target DNA.[27] Plasmonic-based biosensors were used successfully at the POC.[28]

Received: January 31, 2020
Accepted: April 29, 2020
Published: April 29, 2020

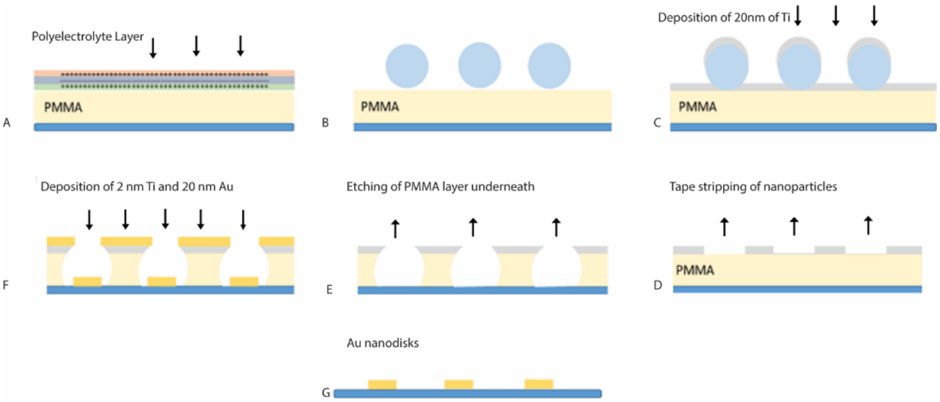

Figure 1. Hole-mask colloidal lithography. The schematic illustrates the fabrication process for creating arrays of gold nanodisk. (A) PMMA layer deposited on a silica substrate coated with a charged polyelectrolyte triple layer; (B) self-assembly of colloidal polystyrene particles onto the surface;. (C) deposition of 20 nm of Ti as a mask layer; (D) tape stripping of the deposited particles; (E) etching of the PMMA layer underneath the holes; (F) deposition of Ti (adhesion layer) and then Au to create structures; and (G) final surface with Au nanodisk arrays after lift off.

Typically LSPR sensors have been exploited to detect biomolecules which match well to the small detection volume of the metallic nanoparticles and can be applied to detect molecular components of bacteria[25] but have also been applied to detect intact viruses and bacteria.[29−31] One approach utilizes nanoparticles adhered to bacteria and consequent surface enhanced Raman spectroscopy read out,[32] another detects aggregation of nanoparticles the surface of bacteria[33] and represent batch processes for the detection of bacteria. The use of refractive index measurements rather than spectroscopic enhancement or aggregation assays has the potential to provide a more quantitative comparison, albeit often with a relatively poor detection limit. In all LSPR approaches, the localization of the sensitive region close to the metal surface limits the types of molecular detection systems that can be used. The use of lithographically surface attached particle allows the tuning shape and size giving control over the extent of the nearfield and spectral position[34] which can enhance sensitivity.[35]

In this study, we have developed a simple, portable, and label-free optical sensor via an aptamer recognition of *S. aureus* at nanostructured plasmonic elements. We optimized the sensor performance via lithographic control, showing a better outcome for larger plasmonic elements (200 vs 100 nm) and compare experiments to simulations of optical response (finite-difference time-domain—FDTD) for different designs specifically addressing the role of the near-field and intrinsic refractive index sensitivity. By tuning the detection readout to the near-infrared, a good sensor performance in a food matrix (milk) was demonstrated which has potential to be applied in a critical control point (CCP) evaluation of bacterial contamination levels.

EXPERIMENTAL METHODS

Materials. Glass coverslips (#2.25 mm diameter and 25 × 60 mm) were purchased from Menzel-Glaser (Germany). PMMA A4 (polymethylmethacrylate) MW 495,000, at 4% concentration in anisole was purchased from Micro resist technology GmbH (Germany). PDDA (poly(dimethylammonium chloride)) and PSS (poly(sodium-4-styrenesulfonate)) were purchased from Sigma-Aldrich (DK). PAX-XL60 (polyammonium chloride) was purchased from Kemira Miljo (DK) and sulphate-modified polystyrene colloidal particles of 100 nm or 200 nm in water were purchased from Invitrogen, sulfur *N*-hydroxysuccinimide (S-NHS), 16-mercaptoundecanoic acid, (TCEP) tris(2-carboxyethyl)phosphine hydrochloride, (6-mercapto-1-hexanol), *N*-(3-dimethylaminopropyl)-*N*-ethylcarbodiimide (EDC), and protein A were purchased from Sigma-Aldrich (DK). Ibidi sticky-Slide VI 0.4 were purchased from Ibidi Germany. Anti-*S. aureus* mouse monoclonal antibody (ab37644) was purchased from Abcam.

The following DNA aptamers sequences were ordered from Metabion, Germany.

Specific aptamer for *S. aureus*: sequence: 5′-thiol-C6-TCC CAC GAT CTC ATT AGT CTG TGG ATA AGC GTG GGA CGT CTA TGA-3′,[36] (no. bases: 45) & *E. coli*: sequence: 5′-thiol-C6-ACG GCG CTC CCA ACA GGCCTC TCC TTA CGG CAT ATT A-3′, (no. bases: 37) *S. aureus* ATCC 8325-4, *Bacillus subtilis* DSM-10 and *E. coli* strain ATCC 8739 (Crooks strain) were used in all experiments.

Methods. *LPSR-Apta Sensor Design.* A first sensor design has made use of a combination of lithographically produced gold nanodisks prepared by colloidal lithography and a DNA aptamer recognition unit.

Nanostructure Fabrication. Gold disks with a nominal diameter of 100 or 200 nm are deposited onto glass slides using a standard hole-mask colloidal lithography (HMCL) method[37] as illustrated in Figure 1. Briefly, the glass substrates were cleaned with an acetone treatment followed by exposure to oxygen plasma (100 W, 25 mTorr for 15 min, Vision 300 Mark II, Advanced Vacuum AB Sweden). The cleaned samples were spin-coated with a 4% solution of PMMA in anisole at 3000 rpm followed by 2 min on a hot plate at 180 °C to produce an approximately 160 nm thick film. The surface of the polymer was given a net positive surface charge by coating with three sequentially deposited polyelectrolyte layers (PDDA, PSS, PAX). A colloidal monolayer of negatively charged polystyrene particles (sulphate modified) of 100 or 200 nm size was then deposited onto the polymer layer by electrostatic self-assembly (100 nm particles, 0.2% in deionized water, 60 s incubation time; 200 nm particles 0.2% concentration in deionized water, and 30 min incubation time). A metal hole mask was formed by the deposition of 20 nm Ti by physical vapour deposition (PVD) (Cryofox GLAD, Polyteknik A/S DK, deposition rate 0.2 Å/s, base pressure $<10^{-7}$ Torr), followed by the removal of the particles by tape stripping. The samples were then etched for 10 min in oxygen plasma ((50 W and 25 mTorr) to remove the PMMA layer below the holes in the hole mask. Subsequently, 20 nm of gold with a 2 nm Ti adhesion layer was deposited through the hole mask by PVD (deposition rates 0.5 Å/s for Ti and 1 Å/s for Au, base pressure $<10^{-7}$ Torr) followed by lift-off in acetone. Finally, the samples were dried under flowing N_2 gas and cleaned via UV/ozone (minimum 30 min in a home built UV/ozone oven) followed by immersion for 1 h in deionized water to reduce the oxidized old generated during UV/ozone treatment back to gold metal. Scanning electron microscopy (Magellan TM XHR SEM, FEI) was used to characterize the samples and determine the disk size and inter-disk distances. AFM (Bruker Dimension Edge) was used to

https://dx.doi.org/10.1021/acsabm.0c00110
ACS Appl. Bio Mater. XXXX, XXX, XXX−XXX

check the heights of the disks. UV/vis spectrophotometry was carried out, (Shimadzu 3300, Shimadzu Japan) to monitor the optical extinction of the nanostructures from 500 to 900 nm wavelength for 100 nm Au disks and from 600 to 1400 nm wavelength for 200 nm Au disks.

Examination of the *S. aureus* Aptamer Specificity. In the developed flow-based sensing system, bacterial strains were identified using the aptamer as a recognition linker between the cells and the sensing elements of the gold nanodisks. A homogeneous gold-coated surface was functionalized with a specific aptamer to examine the specificity of the *S. aureus* aptamer.

Glass substrates of 25 × 60 mm 0.13−0.16 mm standard thickness (Hounisen) were first cleaned with ethanol and then oxygen plasma (100 W, 25 mTorr for 15 min), and then the surface was coated with a 15 nm Au layer with a 2 nm Ti adhesion layer by PVD as before. The substrate was mounted with an Ibidi 6-channel "sticky slide" flow-cell system. *S. aureus* aptamer (100 μL;20 μM) in phosphate-buffered saline (PBS) was added into two channels of the Ibidi flow-cell and incubated under static conditions overnight. *S. aureus*, at a concentration of 10^8 CFU/mL, was introduced into one-channel prefunctionalized with the *S. aureus*-specific aptamer and into another channel with bare gold. Meanwhile, *E. coli* at a concentration of 10^8 CFU/mL was introduced into a channel previously functionalized with the *S. aureus*-specific aptamer, all surfaces were exposed to the bacterial cell innoculates for 30 min. The attached cells were imaged by fluorescence microscopy and counted using ImageJ software.

Self-Assembly of the Aptamer Sensing Layer onto the LSPR Nanostructures. Smaller pieces (25 mm diameter) of the fabricated sensor chips were introduced into a homemade flow system allowing in situ optical characterization. The flow chamber consisted of two-glass sided walls in a holder with one side being the LSPR chip. A syringe pump controlled the flow rate of PBS. Extinction spectra (350−1050 nm) were measured through a ∼1 mm thick chamber using a fiber optic-based light source and spectrometer (B&W Tek Germany). Before introducing the thiolated aptamer to the system, it was necessary to reduce the disulfide to obtain the free thiol from the disulfide. TCEP has been used, which reduces the thiols for each of the aptamer and the backfilling molecule, that is, aptamer−linker−SH and HS−$(CH_2)_6$OH.[38,39] Therefore, 20 μL of 10 μM TCEP hydrochloride was mixed with a 200 μL aptamer solution for 1 h to break the sulfide bond allowing conjugation directly to the gold nanodisks. Afterward, the 200 μL of the *S. aureus* aptamer was injected to the flow chamber and incubated under static conditions. Different incubation times (1, 2, 3, 4 h, and overnight) were examined and the optical spectra were measured after each incubation time to optimize the aptamer immobilization. To remove the nonspecifically adsorbed aptamers, 200 μL 10 μM 6-mercapto-1-hexanol in PBS was injected to the flow chamber and incubated for 30 min under static conditions in order to backfill the surface and orient the DNA aptamer. Afterward, the surface was rinsed gently for 3 min with a 1.50 mL/h flow of PBS, and optical spectra were measured.

Preparation of Bacterial Cultures. Cultures were stored in 30% glycerol at −80 °C and streaked on to 3.7% tryptic soy agar (TSA), incubated at 37 °C until colonies appeared, and re-streaked on TSA to obtain single colonies. A single colony was inoculated from TSA to tryptic soy broth in Erlenmeyer flasks and incubated overnight at 37 °C and 180 rpm/min. Then next day, 1 mL of the culture was centrifuged at 5000*g* for 10 min, followed by the removal of the supernatant. PBS (1 mL) was added and the tube was centrifuged for 10 min at 2000*g* to rinse the cell pellet. PBS was added to re-suspend the pellet to an optical density at (OD600) to 0.1.

Surface Functionalization and Bacterial Cell Detection. The functionalized sensor chip in the flow chamber was exposed to the mentioned concentration of bacterial cells under flow (1.50 mL/h), the optical spectra were measured after 30 and 60 min.

FDTD Simulation of the Optical Response of the Nanodisks. Simulations were carried out with a FDTD solver from Lumerical Solutions (Canada). The Au dielectric function was taken from Johnson & Christy,[40] the organic layers and glass substrate were each approximated by a constant refractive index. A mesh size of 2 × 2 × 2 nm was used and the simulated area was surrounded by a cube of perfectly matched layers, this boundary condition was applied to take into account the absence of long-range ordering in the arrays, which is intrinsic for the sparse colloidal lithography fabrication approach. The peak position of the LSPR resonances was measured by estimating the center of mass of the top 10% of the peak.

Assay Procedure and Sensitivity Test with a Pure Culture of *S. aureus*. Various concentrations of serially diluted cell cultures (10^3, 10^4, 10^5, 10^6, 10^7, and 10^8 CFU/mL) of *S. aureus* were used as test samples on the LSPR chip surface (prepared under the optimum conditions) to examine the sensor's LOD.

After the sensor chip was placed into the flow chamber and sealed carefully, the optical spectra were measured in PBS under flow, followed by the injection of 200 μL of the aptamer at 15 μM concentration into the system in static conditions for 4 h, followed by a gentle rinse. To backfill the surface and oriented the aptamer, 200 μL of the co-thiol 10 μM was injected into the chamber for 30 min followed by a quick and gentle rinse as before. From this stage, the optical spectra were measured continuously. Bacteria were introduced to the system using a syringe pump sequentially, from the lowest concentration to the highest concentration (10^3 to 10^8 CFU/mL) for 30 min for each concentration. A rinsing step with PBS was conducted for 3 min between each concentration.

Applicability of LSPR Sensing Chip in Food Trials. To examine the sensor performance in simulated application conditions, commercially sterilized milk samples were diluted with sterile MQ water in a ratio of 1−10 and spiked with bacteria to give different serial concentrations of *S. aureus* (10^3, 10^4, 10^5, 10^6, 10^7, and 10^8 CFU/mL). The LSPR chip was placed and sealed onto the flow chamber and the LSPR spectra were taken in PBS, then the specific aptamer was assembled on the sensor surface as before. A flow of the diluted milk without bacteria was introduced to the system for 30 min to backfill any unspecific binding and set the baseline for measuring bacterial attachment. Each dilution was introduced to a fresh LSPR chip in the system under optimal conditions and the LOD was calculated from the measured LSPR spectra before and after exposure to the different concentrations of bacteria in the diluted milk. Three replicates were examined for each dilution.

Examination of the Sensor Selectivity. A mixture of different bacterial cultures, including equal concentrations of *S. aureus*, *E. coli,* and *B. subtilis,* were mixed into diluted milk for three experiments. The concentration of each bacteria in each experiment was 3.3 × 10^7, 3.3 × 10^5, and 3.3 × 10^3, respectively, giving total concentrations of 10^8, 10^6, and10^4. The mixtures were introduced to the sensor surface that had been modified with the *S. aureus*-specific aptamer. For this particular experiment, the sensor surface was engineered onto rectangle glass coverslips which were then attached to the ibidi multiflow chamber. The sensor was functionalized at optimized conditions with the *S. aureus* aptamer as described earlier, followed by exposure of the surface to the bacterial mixture in milk for 30 min under static conditions, then the surface was rinsed three times with PBS and the cells were stained with SYBR Green I, and then imaged by confocal laser scanning microscopy using a Zeiss LSM700 CLSM, a 488 nm laser for excitation, and a 20× Plan-Neofluar or a 63× Plan-Apochromat NA 1,4 objective for visualization.

Other control experiments were carried out with the sensor chip. The LSPR chip within the flow system was functionalized by the *S. aureus* aptamer. The sensor readout in a flow of milk was compared to the readout after exposure to a flow of *E. coli*-spiked diluted milk at a concentration of 10^8 CFU/mL for 30 min. The LSPR spectra were obtained and the experiment was repeated 3 times. The same experiment was carried out with *B. subtilis*, examining the change in the LSPR peak position based on presenting spiked milk with *B. subtilis* to the sensor chip (n = 1).

Comparison of Aptamer Based and Immune-Based Detection of *S. aureus*. The LSPR chip was functionalized with oriented antibodies against *S. aureus*. As a first step, the LSPR chip was immersed in 2 mM 16-mercaptohexadecanoic acid in ethanol overnight to achieve a well-organized thiol monolayer, followed by ultra-sonicate treatment in ethanol then in deionized water (5 min

https://dx.doi.org/10.1021/acsabm.0c00110
ACS Appl. Bio Mater. XXXX, XXX, XXX−XXX

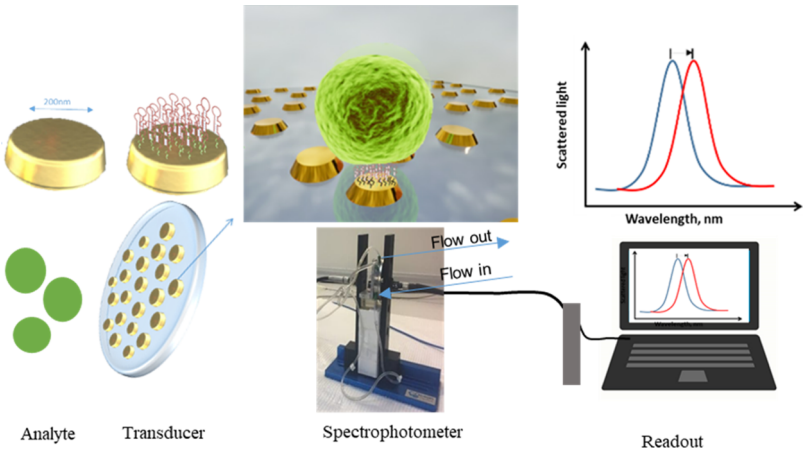

Figure 2. Schematic design of the LSPR platform–based aptamer sensor device. The LSPR spectra shift corresponding to the adsorption of the biomolecule close to the metal surface.

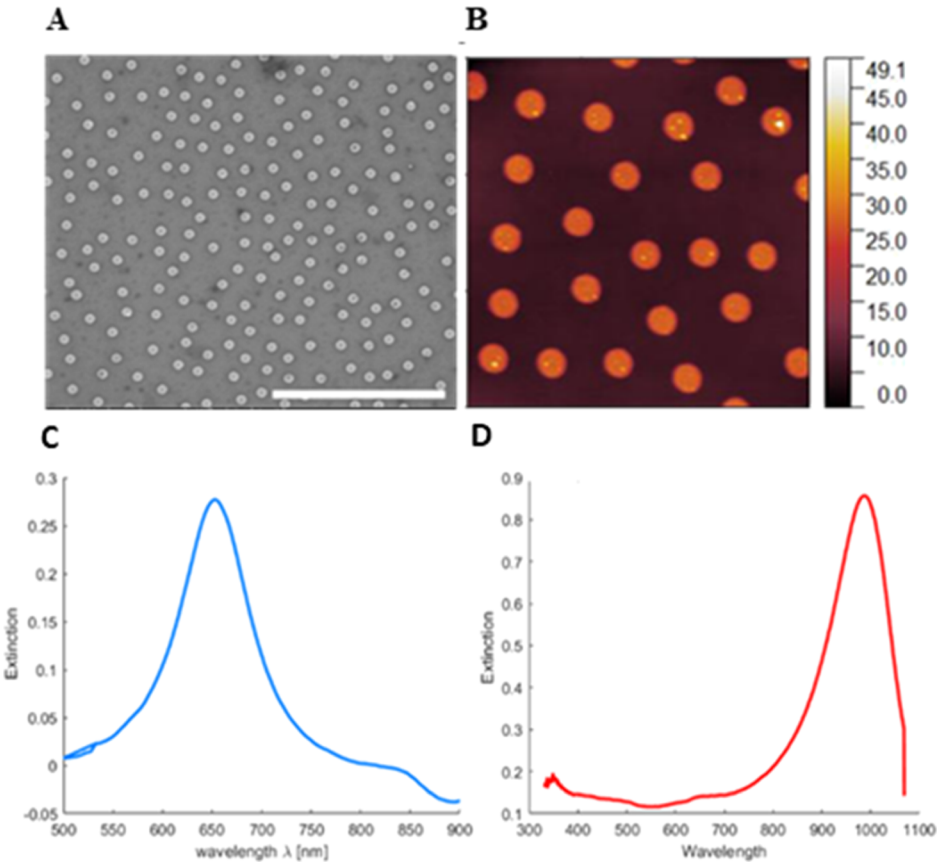

Figure 3. (A,B) SEM and AFM images of 200 nm Au nanodisks. (C,D) LSPR spectra corresponding to 100 and 200 nm disks, respectively. Scale bar = 4 μm.

each) to remove unbound thiols. The chips were then dried under flowing nitrogen. In a subsequent step, the COOH groups of the thiols were activated through aqueous solution of 100 μM MEDAC/50 μM NHS which was added to the chip surface for 10 min followed by rinsing with deionized water, which leads to the formation of NHS-esters. protein A solution (200 mL;25 μg/mL protein A in Ringer's buffer) was injected into the chip under static conditions and incubated for 5 h.[41] The system was rinsed with Ringers buffer then HEPES buffer before injection of 200 μL of 20 μg/mL PLL-*g*-PEG, in HEPES to the surface for 30 min. Flows of *N*-(2-hydroxyethyl)-piperazine-*N*′-ethanesulfonic acid followed by a flow of PBS were used for rinsing. The anti-*S. aureus* antibodies were introduced to the chamber and incubated overnight (concentrations of 20, 50 and 100 μg/mL were studied to optimize the sensor) followed by blocking with BSA 2% in PBS for 30 min. Finally, a flow of *S. aureus* cells (OD600 = 0.1) was exposed to the surface for 30 min. LSPR spectra were obtained before and after exposure to bacteria.

RESULTS AND DISCUSSION

Sensor Chip Design. Arrays of plasmonic gold nanodisks with disk diameters of either 100 or 200 nm, fabricated using the HMCL technique,[18] were employed to enable refractometric detection of *S. aureus*. The general sensing scheme is

https://dx.doi.org/10.1021/acsabm.0c00110
ACS Appl. Bio Mater. XXXX, XXX, XXX–XXX

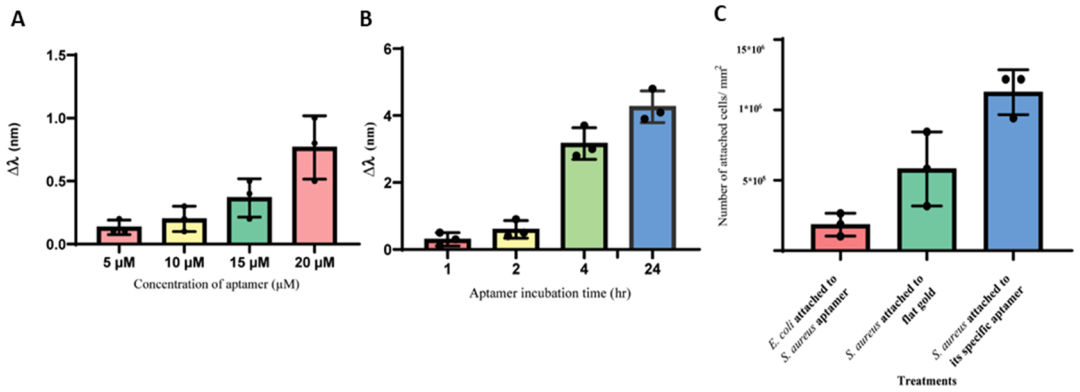

Figure 4. Optimization of conditions for aptamer immobilization at LSPR sensor chips; (A) effect of aptamer concentration on LSPR peak position; (B) effect of aptamer incubation time on the LSPR peak position; and (C) number of *S. aureus* and *E. coli* cells/mm^2 attached to the aptamer or bare gold surface chemistry (error bars show SD n = 3).

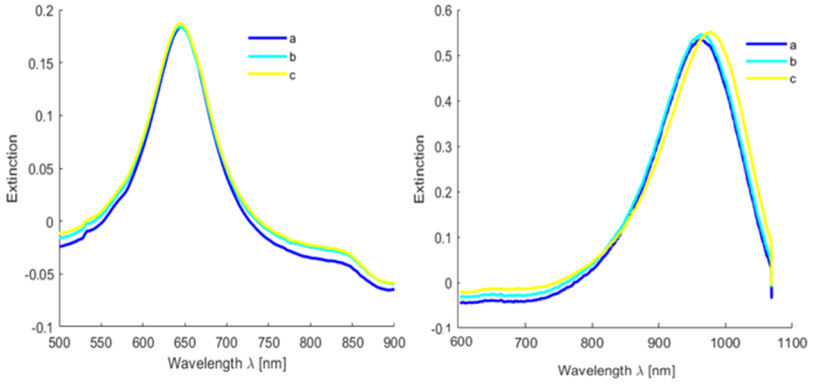

Figure 5. LSPR spectra before and after aptamer deposition and after exposure to *S. aureus* cells for 100 nm disk substrates (left panel) and 200 nm disk substrates (right panel): (a) buffer; (b) DNA aptamer; and (c) *S. aureus* cells.

shown in Figure 2. SEM and an AFM were used for characterization of the disks (Figure 3). The optical spectra of the LSPR of the 100 and 200 gold nanodisks (20 nm height) were measured with a compact custom build fiber spectrometer and showed a maximum absorption peak at 650 nm for the 100 nm disks and 990 nm for the 200 nm disks (under dry conditions).

Sensor Chip Fabrication. LSPRs at plasmonic nanoparticles are sensitive to changes in the dielectric environment surrounding the nanoparticles.[42] Here, we exploit that property as an analytical system for rapid detection of bacteria. The sensor chip was fabricated using HMCL (shown in Figure 1) using the pattern of deposited polystyrene nanoparticles as a mask to fabricate arrays of gold disks of defined diameter and height. In the process colloidal nanoparticles were assembled on top of a thin PMMA layer by electrostatic self-assembly, then a 20 nm thick titanium layer was deposited to form (after particle removal by tape striping) a sacrificial hole mask. Oxygen plasma etching revealed the substrate below the holes and a 20 nm thick gold layer was deposited with a 2 nm titanium adhesion layer. Lift off of the PMMA and hole mask left a short range order gold disk array. The disks have the shape of truncated cones because the hole in the hole mask narrows progressively during the deposition of the titanium adhesion layer and gold layer. The fabricated LSPR chip was functionalized with the *S. aureus* specific DNA aptamers with 45 single-strand oligonucleotides; 5′-thiol-C6-TCCCAC-GATCTCATTAGTCTGTGGATAAGCGTGGGACGTC-TATGA-thiol-3′ as a recognition element to the specific cells.

In the present study, the developed gold nanodisk-aptamer-based LSPR sensing chips were tested for their detection performance against *S. aureus*. The long term perspective is the development of compact sensing devices to reduce detection cost and time with improved sensitivity. Aptamer-functionalized chips were compared to chips functionalized with *S. aureus* antibodies as a recognition linker and proved to have enhanced sensing properties and minimized measurement steps. There are several additional advantages of aptamers, such as easy labeling, long-term stability, and lower cost.

Optimization of Conditions for the Conjugation of Aptamers. To optimize the appropriate concentration and incubation time that is required for conjugation of the aptamer to the fabricated LSPR chip surface, different concentrations of aptamer (5, 10, 15, and 20 μM) and incubation times (1, 2, 3, 4, and 12 h) were examined for the sensor chip surfaces formed with 200 nm diameter gold disks. The optical response of the sensor was used to evaluate the aptamer binding. In response to the change in the thiolated aptamer concentrations, the LSPR peak position changed as the local refractive index increased and displayed the time-resolved binding event.

The thiolated aptamer self-assembles onto the gold surface via the thiol group.[38] Figure 4A,B shows the shift in the LSPR peak position versus aptamer concentration and exposure time. Similar binding was observed for bacterial attachment to homogeneous surfaces functionalized with the aptamer at the 15 and 20 μM conditions so an aptamer concentration of 15 μM was selected to reduce the costs. Four hours was shown to be sufficient for the aptamer to achieve a stable coverage of the

https://dx.doi.org/10.1021/acsabm.0c00110
ACS Appl. Bio Mater. XXXX, XXX, XXX−XXX

gold nanodisks. These conditions were used as an optimal condition for all the following experiments.

The specificity of the aptamer for *S. aureus* was confirmed by comparison of adhesion of *E. coli* and *S. aureus* (OD600 = 0.1, 30 min) to the *S. aureus*-specific aptamer immobilized at homogeneous gold-coated surfaces (20 nm Au with 2 nm Ti adhesion layer). The binding of *S. aureus* to the aptamer was high, while *E. coli* attachment to the aptamer was marginal (Figure 4C) relatively high levels of binding were seen to unfunctionalized gold surfaces, however, LSPR data confirms that aptamer monolayers are assembled at the gold surface.

Assay Procedure and Sensitivity Test with a Pure Culture of *S. aureus* in PBS. The sensor device was placed in a custom-built flow chamber (Figure S3) and flushed with 10× PBS and a base-spectrum was measured. Thereafter, an aptamer layer was assembled under optimum conditions (200 μL of 15 μM aptamer was added and exposed to the chip for 4 h). These conditions allowed the DNA aptamer to become attached to the Au disk surface.[38,39,43,44] The sensor surface was backfilled with a "co-thiol"[38] of 6-mercapto-1-hexanol, to minimize aptamer interaction with gold and give correct orientation. The co-thiol was injected to the surface for 30 min after aptamer immobilization.

Here, we investigated the role of the specific plasmonic structure on the bacterial detection process. Two gold nanostructure designs of height 20 nm and diameter either 100 or 200 nm were compared for enhancing the detection and enlarging the LSPR signal. The two sensor chips were tested in the flow chambers and exposed to a flow of *S. aureus* (OD600 = 0.1, 30 min). Figure 5 shows representative extinction spectra for 100 nm disks (Figure 5 left panel) and 200 nm disks (Figure 5 right panel) in PBS, after aptamer immobilization and *S. aureus* exposure. The response from the large nanostructure was clearly larger. An average shift of ∼4.3 nm standard deviation (SD) 0.8 n = 3] was induced by the aptamer sensor with the larger nanostructures (200 nm), while the chip with the smaller nanodisks (100 nm) induced an average shift of ∼0.6 nm (SD 0.5 nm, n = 5) (Figure 5).

The performance of the sensor chip with the *S. aureus*-specific aptamer recognition layer was compared to an antibody-based *S. aureus* recognition layer. Anti-*S. aureus* IgG was immobilized and oriented at the surface of the gold nanostructures in a multilayer procedure to ensure that the recognition domains of the IgG were presented out from the surface. Protein A was covalently immobilized at a carboxylated thiol monolayer via EDC/NHS coupling and subsequently used to immobilize IgG through binding to the Fc domain (see Figure 6 right panel).

The performance of the antibody-based sensor was poor (Figure S4). With a zero response for the detection of *S. aureus* (even showing a blue shift) for the immunosensor based on 100 nm disks for and a small ∼0.5 nm shift for the sensor based on 200 nm nanodisks. The response was low despite the presence of bacteria attached at the sensor surfaces. We cannot rule out that different binding strengths of the antibody versus the aptamer could have contributed to the difference in signal.

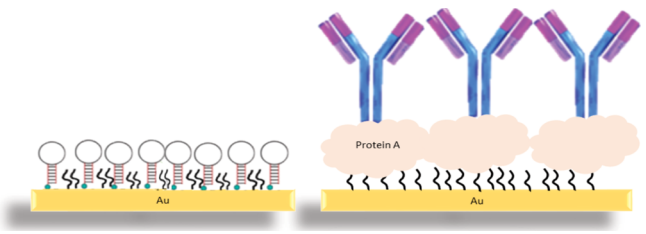

Figure 6. Schematic representation of the sensing layers at gold surfaces: aptamer (left panel) and multilayer of alkanethiol/protein A/IgG (right panel).

FDTD Simulation of Optical Response of the Nanodisks. To understand the dependence of the LSPR optical response on different nanostructure sizes and shapes and in the presence of different recognition layers, we performed FDTD simulations. FDTD is one of the most commonly applied numerical methods in plasmonics. Figure 7a shows a schematic of the expected sizes of the Au-APTA sensor and bacteria and a 200 nm diameter nanodisk. In the aptamer-based sensor, the immobilized layer of the DNA aptamer was represented by a 6 nm thick layer (6.2 nm for an aptamer loop attached to the surface at both ends and somewhat compressed (45 bp/2) × 0.36 nm per bp × 0.70 for compression also including the ∼0.6 nm C6 spacer and thiol but was represented as 6 nm in the 2 nm resolution FDTD model). For the immunosensor, the IgG presenting layer was represented by a 20 nm thick layer (12 nm for IgG + 6 nm for protein A + 2 nm thiol layer). The *S. aureus* cell was represented by a sphere of 1 μm in size but in contact with the complete upper layer of the nanodisk. The calculated field distributions for the two sizes of the disk at the resonant wavelength are shown in Figure 7B,C. The changes in the refractive index sensitivity for different steps in the experiment were estimated in the FDTD model by adding layers of higher refractive index and assuming the refractive index of the DNA aptamer layer to be 1.5 (assuming a mix of single, double-stranded DNA segments,[45] and two alkyl spacers), the protein layer to be 1.343[18] and that representing the bacteria to be 1.39.[46] This simulation resulted in a redshift for 100 nm disks ∼10.5 and 5.8 nm for the DNA aptamer layer and full bacterial cells, respectively. While, in 200 nm disks, the wavelength shift with the addition of DNA and bacteria was 12.1 and 10.3 nm, respectively. The simulations gave significantly larger peak shifts than that found experimentally, but it should be remembered that not every disk will have an adhered bacterium and the attachment can be at several locations on a disk or even between disks by being attached to two or more disks. The FDTD simulation gave somewhat different peaks of shapes and position from the experimental peaks for both Au nanodisks with a diameter of 100 and 200 nm. The simulated structure is one specific size and shape while the experimental sample represents a distribution of sizes and aspect ratios, however, the difference between the two sizes can be seen. The FDTD simulations confirm the experimental data and show that the larger diameter disks have resonances at longer wavelengths and have a larger shift from both the DNA layer and the bacterium. The field plots, as shown in Figure 7B,C, show that the Au nanodisks with 100 nm diameter have a shorter range sensing field (see the extent of the green part of the field) compared to the 200 nm structures which means that a smaller fraction of the bacteria is placed within the sensitive region of the smaller disks. The higher sensitivity for the larger disks is likely a combination of the larger bulk refractive index sensitivity for disks with longer wavelength resonances and the larger extent of the field.

The FDTD simulations indicated that the use of the DNA aptamer has an advantage over the antibodies for LSPR sensors based on both 100 and 200 nm Au disks in terms of the peak shift resulting from bacterial adhesion. The spectral shift

https://dx.doi.org/10.1021/acsabm.0c00110
ACS Appl. Bio Mater. XXXX, XXX, XXX−XXX

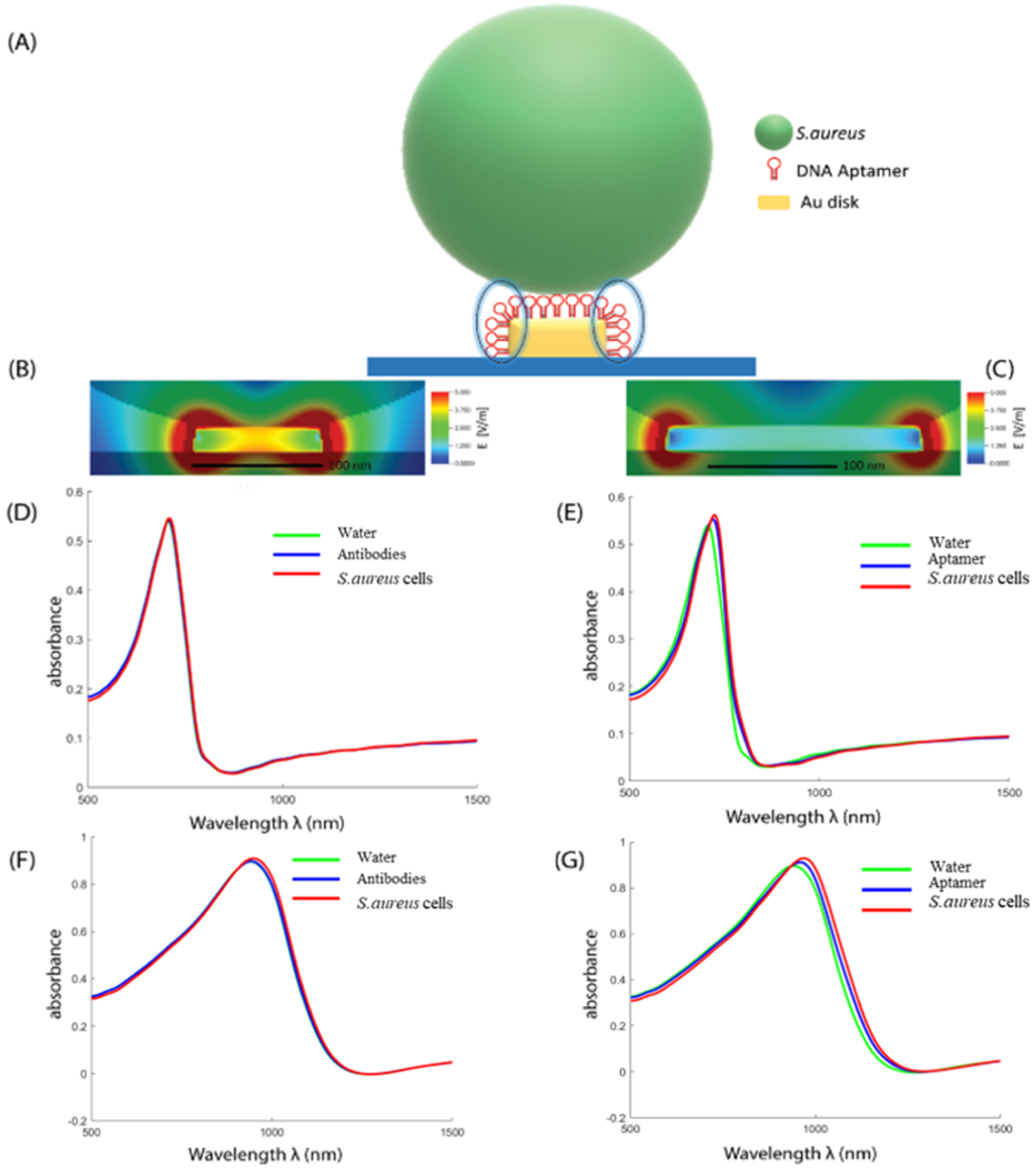

Figure 7. Schematic representation of the LSPR-aptasensor expected mechanism (A). Field enhancement distribution image of the cross section along the center of the 100 nanostructure in (B) and 200 nm structure in (C). FDTD simulation based on sensor device with 100 nm fabricated nanodisks with antibodies as biorecognition elements in (D); aptamer in (E); 200 nm fabricated nanodisks functionalized with antibodies in (F); and 200 nm Au disks functionalized with aptamer (G).

corresponding to bacterial attachment was increased by 380% when the antibodies were replaced by DNA with the 100 nm disks moving from 1.2 nm (704.9−706.1 nm), in the case of antibody-based detection, to 5.8 nm (713.2−719 nm) for DNA aptamer recognition and by 70% with the 200 nm Au disks with a spectral shift of 6 nm with antibodies (from 933.8 to 939.8 nm) after adding bacteria, in contrast to the case of aptamer immobilization and the spectral shift of 10.3 nm after bacterial attachment (945.8−956.1 nm). The significant increase in sensitivity to bacterial attachment for the aptamer layer compared to the antibody layer correlates to the significantly thinner extent of the aptamer recognition layer (6.2 nm estimated as 6 nm in the simulation) compared to the antibody-based recognition layer (20 nm). Figure 6 schematically shows the relative thickness of the two recognition layers. The sensing region of the LSPR is close to the nanoparticle surface and the antibody-based recognition layer is sufficiently thick to lift the sensing event of the bacterial attachment substantially outside of this sensing region. The sensing region is larger for larger nanodisks as the optical near-field associated with the plasmon extends further from the metal surface, and there is a larger part of the sensitive detection volume for detection using the antibody system for the larger disks compared to the smaller disks. Alternative routes to attach the antibody to the surface could reduce the thickness of this layer, for example, through direct coupling to the surface and use of smaller units such as single-chain antibodies or nanobodies. The layer thickness of the sensing layer is a critical parameter in the design of LSPR-based sensor systems.

Assay Procedure and Sensitivity Test for *S. aureus* Detection. Based on the testing carried out, the 200 nm diameter aptamer-based LSPR sensing chips were selected for

https://dx.doi.org/10.1021/acsabm.0c00110
ACS Appl. Bio Mater. XXXX, XXX, XXX−XXX

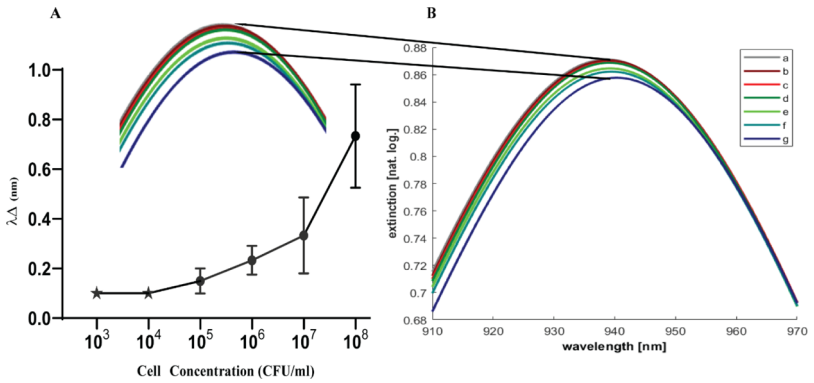

Figure 8. (A) Sensor output corresponding to different *S. aureus* concentrations, (B) representative spectra for the LSPR before and after exposure to different concentrations of *S. aureus* cells [(a) aptamer, (b) 10^3, (c) 10^4, (d) 10^5, € 10^6, (f) 10^7, and (g) 10^8 CFU/mL]. Error bars show SD (n = 3—except for starred which are single measurements).

exploration in bacterial detection. The sensitivity and LOD was measured using serially diluted cell cultures (10^3,10^4, 10^5, 10^6, 10^7, and 10^8 CFU/mL) of *S. aureus*. Figure 8b shows representative extinction spectra obtained for different concentrations and average peak position shifts was determined.

The LSPR peak position shifted to longer wavelengths with increasing concentrations up to approximately 10^7 CFU/mL (Figure 8A,B), suggesting the good quantification capability in the linear-log detection range with a LOD of 10^3 CFU/mL. *S. aureus* induced a significantly larger LSPR peak shift at a concentration of 10^8.

Applicability of LSPR Sensing Chip in Food Trials. To confirm the practical applicability of the developed sensor chip, detection of bacteria in milk was evaluated. Commercially sterilized milk samples were spiked with different serial concentrations of *S. aureus* cells (10^3, 10^4, 10^5, 10^6, 10^7, and 10^8 CFU/mL). Each dilution was introduced to the system and the LOD was tested by the LSPR. The sensor showed a linear response with a log scale increase of bacteria up to around 10^6 CFU/mL, above which the signal increased more rapidly. The detection limit in the selected food matrix was similar to that in the pure culture system (Figure 9), indicating

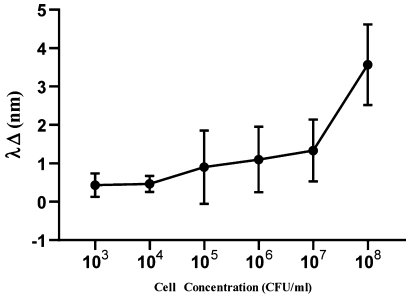

Figure 9. LSPR peak position shift for the detection of different *S. aureus* concentrations (CFU/mL) in milk. Error bars show SD, n = 3.

that the developed method is robust and unhindered by competing molecules in the milk samples. The real-time measurements were taken for milk samples inoculated with *S. aureus* to a concentration of 10^8/mL. The experiment revealed that the change of LSPR spectral was achieved rapidly (in around 120 s) after the milk sample was injected into the flow system (Figure 10).

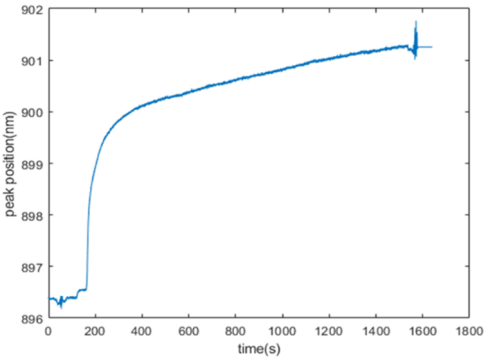

Figure 10. Real-time measurement of a diluted milk sample that was spiked with 10^8 CFU/mL *S. aureus* cell concentration. The spiked milk sample was injected into the flow after 30 min of milk flow shown as at 60 s and the shift occurred at 180 s.

The number of bacteria binding to the sensor surface from milk under different concentrations was confirmed by fluorescent microscopy. Here, the sensor device was fabricated onto a rectangular coverslip 25 × 60 mm and applied to a commercial (ibidi chamber) fluidic channel to allow the introduction of bacteria and exposure under static conditions.

Three different *S. aureus* cell concentrations 10^8, 10^6, and 10^4 CFU/mL were injected to the ibidi channels and incubated for 30 min under static conditions. The attached cells were subsequently imaged by confocal microscopy and counted by ImageJ to confirm that the sensor device responses to the varied cell concentrations in a various methods agreed with the spectral measurements (Figure 11).

Examination of the Sensor Selectivity. The first test was done to explore if the *S. aureus* could bind to the aptamer surface in the presence of other bacteria. A mixture of 3 different bacterial cells (*S. aureus, E. coli* and *B. subtilis*) was prepared in the milk sample with equal concentrations of each bacteria to give 10^8, 10^6, and 10^4 CFU/mL as final concentrations. Figure 12A shows images of SYBR Green I labeled bacteria attached to the *S. aureus* aptamer-coated sensor surfaces. The *S. aureus* can be distinguished from the other bacteria by its spherical shape and almost no *E. coli* and *B. subtilis* were identified.

The sensor selectivity was studied by comparison of the binding of *E. coli* and *B. subtilis* to the sensor surface functionalized with the aptamer against *S. aureus*. Separate experiments were carried out for both *E. coli* and *B. subtilis* in

https://dx.doi.org/10.1021/acsabm.0c00110
ACS Appl. Bio Mater. XXXX, XXX, XXX−XXX

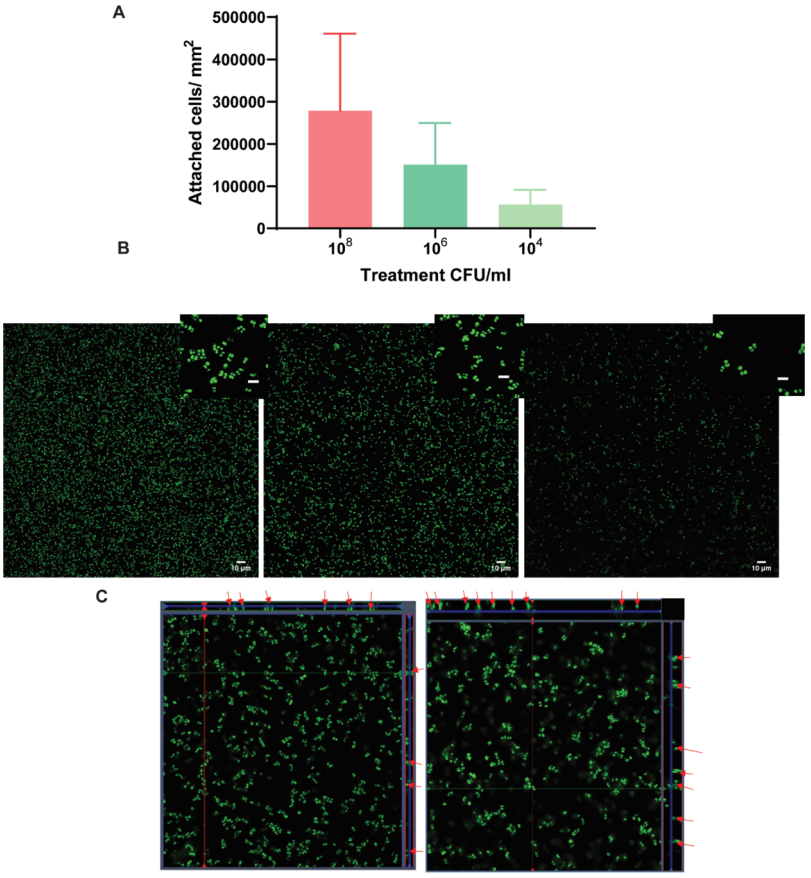

Figure 11. (A) Number of attached cells onto the sensor surface/mm^2, error bars show SD, n = 3 and three images were taken from each sample; (B) confocal images taken at 20× visualizing the attached *S. aureus* cells on the sensor device (left 10^8 CFU/mL, center 10^6 CFU/mL, right 10^4 CFU/mL), scale bar is 10 μm in all images, the inset images were taken at 63× (C) orthogonal view of the attached *S. aureus* cells onto the sensor surface, cells attached at the surface were highlighted with arrows. Objective 63× and the scale bar is 10 μm.

parallel, the milk sample was spiked by each bacteria separately with a concentration of 10^8 CFU/mL then it was exposed to the sensor surface for 40 min and showed only a minor peak shift in the LSPR position (see Figure 12B LSPR shift 0.2 nm with SD = 0.04 n = 3 & Figure 12C LSPR shift for 0.14 nm).

Repeatability and Reliability of the Sensor. The sensor chips were produced from several production batches which showed a maximum absorption peak at 650 nm for the 100 nm disks and 990 nm for the 200 nm disks (under dry conditions) with a variation of around ±10 nm between batches. This variation in peak position results from material fabrication issues, such as polymer and metal film thickness during processing, and can likely be improved. This level of peak position variation will only vary by a few percent in the refractive index sensitivity.

Advantages of the Device. Milk and its products are implicated in staphylococcal food poisoning (SFP)[47] as raw milk can be contaminated as a result of *S. aureus* mastitis, which poses a serious problem in dairy. *S. aureus* causes SFP.[48,49] *S. aureus* or its enterotoxins might remain even in pasteurized milk and a level of 500,000−1,000,000 *S. aureus* cells per gram is needed for the *S. aureus* toxin to reach levels that cause food poisoning.[48] However, levels of *S. aureus* organisms in raw milk or other dairy products equal to 10^4CFU/mL are indicators of a lack of sanitary conditions and risk of contamination.[50] Therefore, identification of the level of *S. aureus* in milk during the production process is considered a CCP for this hazard.

The LSPR-Apta sensor based on 200 nm diameter nanodisks, developed in this study, produced an LSPR detection measurement of *S. aureus* in less than 5 min and could quantify within 30 min. The developed sensor chip can be used as a portable detector for evaluating and monitoring the CCP through bulk milk production steps with a LOD of 10^3 CFU/mL for controlling the hazards and improving safety standards for hindering SFP.

Other developed approaches such as via PCR amplification of bacterial DNA have been shown to detect lower levels of *S. aureus* (e.g. 10^2 CFU/mL in shrimp homogenate spiked with pure culture after enrichment for 6 h[51]) but take longer times or require more complicated processes. The LSPR system is instrumentally simpler than many other sensing devices such as SPR, as the instrument consists only of a light source, a chamber, and a detector and has the potential for online detection with short detection times (down to 120 s). The localized sensing of the approach means that the bulk refractive index gives negligible effects compared to the signal.

CONCLUSIONS

In this work, we carry out the proof of principle studies of the response of an LSPR as a label-free sensor for bacteria detection. A DNA aptamer was used as a recognition element to capture bacteria within the local optical field of an optically active metal nanostructure and provide a colorimetric readout. The gold nanodisks were fabricated on a glass substrate by a parallel self-assembly based patterning approach (HMCL). A

https://dx.doi.org/10.1021/acsabm.0c00110
ACS Appl. Bio Mater. XXXX, XXX, XXX−XXX

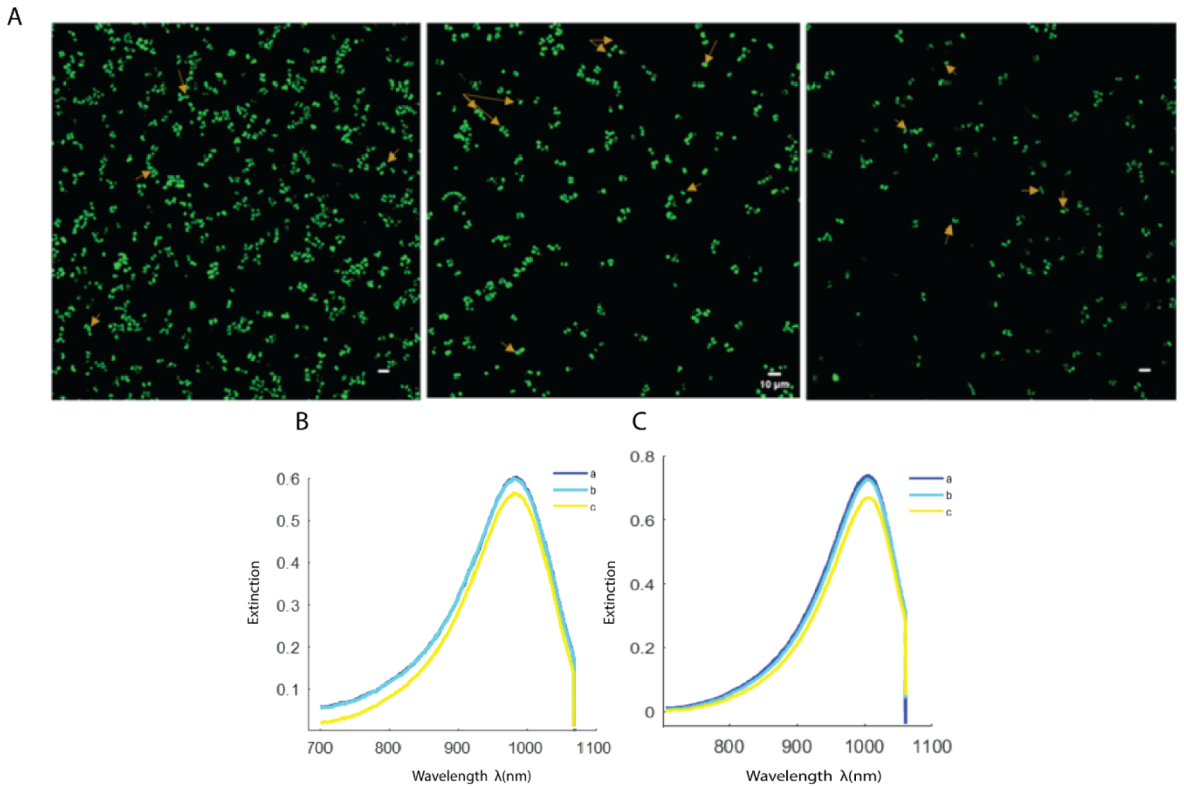

Figure 12. (A) Confocal images for surfaces exposed to mixed cell cultures (*S. aureus*, *E. coli*, and *B. subtilis*) with three different concentrations 10^8, 10^6; and 10^4, showing that almost only *S. aureus* cells were attached (the arrows point to the nonspherical shapes that may indicate small numbers of *E. coli* and *B. subtilis*). (B,C) LSPR spectra of 200 nm disks before and after exposure to the aptamer and after exposure to *E. coli* or *B. subtilis* cells respectively, with a very limited peak shift ∼0.2 nm n = 3, SD = 0.06 n = 3 for *E. coli* and 0.14 for *B. subtilis* n = 1 (a = PBS, b = aptamer = *E. coli* cells).

comparison of the aptamer to antibody-based recognition approaches indicated that the thickness of the sensing layer was critical with a significantly larger response for the thinner aptamer layer. Comparison of the differently sized metal nanostructures showed a significantly higher sensitivity for 200 nm diameter compared to 100 nm diameter disk structures resulting from both increases in the bulk refractive index sensitivity and the extent to which the local field extends out from the metal surface.[52,53] These experimental results were confirmed by FDTD electrodynamic calculations of the sensing response for different layer thicknesses and different nanostructures. Finally, the sensor performance was demonstrated in a complex food matrix (milk). This developed sensor platform has the potential for application as a compact bacterial sensor in food production systems.

■ ASSOCIATED CONTENT

Supporting Information

The Supporting Information is available free of charge at https://pubs.acs.org/doi/10.1021/acsabm.0c00110.

SEM images of disks and bacterial adhesion data from the optimization of the aptamer orientation (PDF)

■ AUTHOR INFORMATION

Corresponding Author

Duncan S. Sutherland − *Interdisciplinary Nanoscience Center (iNANO), Aarhus University, 8000 Aarhus C, Denmark;* orcid.org/0000-0002-5045-9915; Email: duncan@inano.au.dk

Authors

Heba Khateb − *Interdisciplinary Nanoscience Center (iNANO), Aarhus University, 8000 Aarhus C, Denmark;* orcid.org/0000-0002-9166-8991

Gunnar Klös − *Interdisciplinary Nanoscience Center (iNANO), Aarhus University, 8000 Aarhus C, Denmark;* orcid.org/0000-0002-7112-8621

Rikke L. Meyer − *Interdisciplinary Nanoscience Center (iNANO), Aarhus University, 8000 Aarhus C, Denmark*

Complete contact information is available at: https://pubs.acs.org/10.1021/acsabm.0c00110

Author Contributions

The manuscript was written through contributions of all the authors. All the authors have given approval to the final version of the manuscript.

Notes

The authors declare no competing financial interest.

■ ACKNOWLEDGMENTS

This work was supported by the Independent Research Fund Denmark through the grant DFF-4184-00301 and Danish National Research Foundation grant CellPAT (DNRF135). Affiliation with the center for integrated materials research (iMAT) at Aarhus University is acknowledged.

■ REFERENCES

(1) Nyachuba, D. G. Foodborne illness: Is it on the rise? *Nutr. Rev.* **2010**, *68*, 257−269.

(2) Velusamy, V.; Arshak, K.; Korostynska, O.; Oliwa, K.; Adley, C. An overview of foodborne pathogen detection: In the perspective of biosensors. *Biotechnol. Adv.* **2010**, *28*, 232−254.
(3) Brugha, R.; Vipond, I. B.; Evans, M. R.; Sandifer, Q. D.; Roberts, R. J.; Salmon, R. L.; Caul, E. O.; Mukerjee, A. K. A community outbreak of food-borne small round-structured virus gastroenteritis caused by a contaminated water supply Epidemiol. *Epidemiol. Infect.* **1999**, *122*, 145−154.
(4) Oh, S. Y.; Heo, N. S.; Shukla, S.; Cho, H.; Vilian, A. T. E.; Kim, J. Development of gold nanoparticle- aptamer-based LSPR sensing chips for the rapid detection of Salmonella typhimurium in pork meat. *Sci. Rep.* **2017**, *7*, 10130.
(5) Zhang, P.; Liu, H.; Ma, S.; Men, S.; Li, Q.; Yang, X.; Wang, H.; Zhang, A. A label-free ultrasensitive fluorescence detection of viable Salmonella enteritidis using enzyme-induced cascade two-stage toehold strand- displacement-driven assembly of G-quadruplex DNA. *Biosens. Bioelectron.* **2016**, *80*, 538−542.
(6) Tranter, D. Foodborne staphylococcal illness. *Lancet* **1990**, *336*, 1044−1046.
(7) Hirooka, E. Y.; De Salzberg, S. P. C.; Bergdoll, M. S. Production of staphylococcal enterotoxin A and thermonuclease in cream pies. *J. Food Prot.* **1987**, *50*, 952−955.
(8) de Oliveira, L. P.; e Barros, L. S. S.; Silva, C. V.; Cirqueira, M. G. Study of Staphylococcus aureus in raw and pasteurized milk consumed in the Reconcavo area of the State of Bahia, Brazil. *J. Food Process. Technol.* **2011**, *02*, 1000128.
(9) Capparelli, E.; Mata, L. Microflora of Maize Prepared as Tortillas Microflora of Maize Prepared as Tortillas. *Appl. Environ. Microbiol.* **1975**, *29*, 802−806.
(10) do Carmo, L. S.; Dias, R. S.; Linardi, V. R.; Sena, M. J. d.; Santos, D. A. d. An outbreak of Staphylococcal food poisoning in the municipality of Passos, Mg, Brazil. *Braz. Arch. Biol. Technol.* **2003**, *46*, 581−586.
(11) *Microbial Safety of Minimally Processed Foods*; Novak, J. S., Sabers, G. M., Juneja, V. K., Eds.; CRC Press, 2003; pp 4−11.
(12) Daly, P.; Collier, T.; Doyle, S. PCR-ELISA detection of Escherichia coli in milk. *Lett. Appl. Microbiol.* **2002**, *34*, 222−226.
(13) Kralik, P.; Ricchi, M. A Basic Guide to Real Time PCR in Microbial Diagnostics: Definitions, Parameters, and Everything. *Front. Microbiol.* **2017**, *8*, 108.
(14) Liao, J. C.; Mastali, M.; Li, Y.; Gau, V.; Suchard, M. A.; Babbitt, J.; Gornbein, J.; Landaw, E. M.; McCabe, E. R. B.; Churchill, B. M.; Haake, D. A. Development of an Advanced Electrochemical DNA Biosensor for Bacterial Pathogen Detection. *J. Mol. Diagn.* **2007**, *9*, 158−168.
(15) Wang, Y.; Ye, Z.; Ying, Y. New Trends in Impedimetric Biosensors for the Detection of Foodborne Pathogenic Bacteria. *Sensors* **2012**, *12*, 3449−3471.
(16) Waswa, J.; Irudayaraj, J.; Debroy, C. Direct detection of E . Coli O157: H7 in selected food systems by a surface plasmon resonance biosensor. *LWT—Food Sci. Technol.* **2007**, *40*, 187−192.
(17) Lv, X.; Geng, Z.; Su, Y.; Fan, Z.; Wang, S.; Fang, W.; Chen, H. Label-Free Exosome Detection Based on a Low-Cost Plasmonic Biosensor Array Integrated with Microfluidics. *Langmuir* **2019**, *35*, 9816−9824.
(18) Guerreiro, J. R. L.; Frederiksen, M.; Bochenkov, V. E.; De Freitas, V.; Ferreira Sales, M. G.; Sutherland, D. S. Multifunctional Biosensor Based on Localized Surface Plasmon Resonance for Monitoring Small Molecule-Protein Interaction. *ACS Nano* **2014**, *8*, 7958−7967.
(19) Yoo, S. M.; Kim, D.-K.; Lee, S. Y. Talanta Aptamer-functionalized localized surface plasmon resonance sensor for the multiplexed detection of different bacterial species. *Talanta* **2015**, *132*, 112−117.
(20) Wang, X.; Li, Y.; Wang, H.; Fu, Q.; Peng, J.; Wang, Y.; Du, J.; Zhou, Y.; Zhan, L. Gold nanorod-based localized surface plasmon resonance biosensor for sensitive detection of hepatitis B virus in buffer, blood serum and plasma. *Biosens. Bioelectron.* **2010**, *26*, 404−410.
(21) Liu, J.; Jalali, M.; Mahshid, S.; Wachsmann-Hogiu, S. Are plasmonic optical biosensors ready for use in point-of-need applications? *Analyst* **2020**, *145*, 364−384.
(22) Hammond, J.; Bhalla, N.; Rafiee, S.; Estrela, P. Localized Surface Plasmon Resonance as a Biosensing Platform for Developing Countries. *Biosensors* **2014**, *4*, 172−188.
(23) Nagatsuka, T.; Uzawa, H.; Sato, K.; Kondo, S.; Izumi, M.; Yokoyama, K.; Ohsawa, I.; Seto, Y.; Neri, P.; Mori, H.; Nishida, Y.; Saito, M.; Tamiya, E. Localized Surface Plasmon Resonance Detection of Biological Toxins Using Cell Surface Oligosaccharides on Glyco Chips. *ACS Appl. Mater. Interfaces* **2013**, *5*, 4173−4180.
(24) Cottat, M.; Thioune, N.; Gabudean, A.-M.; Lidgi-Guigui, N.; Focsan, M.; Astilean, S.; Lamy de la Chapelle, M. Localized Surface Plasmon Resonance (LSPR) Biosensor for the Protein Detection. *Plasmonics* **2013**, *8*, 699−704.
(25) Chen, S.; Svedendahl, M.; Käll, M.; Gunnarsson, L.; Dmitriev, A. Ultrahigh sensitivity made simple: Nanoplasmonic label-free biosensing with an extremely low limit-of-detection for bacterial and cancer diagnostics. *Nanotechnology* **2009**, *20*, 434015.
(26) Guo, L.; Zhou, X.; Kim, D.-H. Facile fabrication of distance-tunable Au-nanorod chips for single-nanoparticle plasmonic biosensors. *Biosens. Bioelectron.* **2011**, *26*, 2246−2251.
(27) Lednický, T.; Bonyár, A. Large Scale Fabrication of Ordered Gold Nanoparticle−Epoxy Surface Nanocomposites and Their Application as Label-Free Plasmonic DNA Biosensors. *ACS Appl. Mater. Interfaces* **2020**, *12*, 4804−4814.
(28) Li, Z.; Leustean, L.; Inci, F.; Zheng, M.; Demirci, U.; Wang, S. Plasmonic-based platforms for diagnosis of infectious diseases at the point-of-care. *Biotechnol. Adv.* **2019**, *37*, 107440.
(29) Draz, M. S.; Shafiee, H. Applications of gold nanoparticles in virus detection. *Theranostics* **2018**, *8*, 1985−2017.
(30) Zhang, Z.; Wang, H.; Chen, Z.; Wang, X.; Choo, J.; Chen, L. Plasmonic colorimetric sensors based on etching and growth of noble metal nanoparticles: Strategies and applications. *Biosens. Bioelectron.* **2018**, *114*, 52−65.
(31) Adegoke, O.; Morita, M.; Kato, T.; Ito, M.; Suzuki, T.; Park, E. Y. Localized surface plasmon resonance,mediated fluorescence signals in plasmonic nanoparticle-quantum dot hybrids for ultrasensitive Zika virus RNA detection via hairpin hybridization assays. *Biosens. Bioelectron.* **2017**, *94*, 513−522.
(32) Whang, K.; Lee, J. H.; Shin, Y.; Lee, W.; Kim, Y. W.; Kim, D.; Lee, L. P.; Kang, T. Plasmonic bacteria on a nanoporous mirror via hydrodynamic trapping for rapid identification of waterborne pathogens. *Light Sci. Appl.* **2018**, *7*, 68.
(33) Peng, H.; Chen, I. A. Rapid Colorimetric Detection of Bacterial Species through the Capture of Gold Nanoparticles by Chimeric Phages. *ACS Nano* **2019**, *13*, 1244−1252.
(34) Hanarp, P.; Käll, M.; Sutherland, D. S. Optical Properties of Short Range Ordered Arrays of Nanometer Gold Disks Prepared by Colloidal Lithography. *J. Phys. Chem. B* **2003**, *107*, 5768−5772.
(35) Larsson, E. M.; Alegret, J.; Käll, M.; Sutherland, D. S. Sensing characteristics of NIR localized surface plasmon resonances in gold nanorings for application as ultrasensitive biosensors. *Nano Lett.* **2007**, *7*, 1256−1263.
(36) Cao, X.; Li, S.; Chen, L.; Ding, H.; Xu, H.; Huang, Y.; Li, J.; Liu, N.; Cao, W.; Zhu, Y.; Shen, B.; Shao, N. Combining use of a panel of ssDNA aptamers in the detection of Staphylococcus aureus. *Nucleic Acids Res.* **2009**, *37*, 4621−4628.
(37) Guerreiro, J. R. L.; Teixeira, N.; De Freitas, V.; Sales, M. G. F.; Sutherland, D. S. A saliva molecular imprinted localized surface plasmon resonance biosensor for wine astringency estimation. *Food Chem.* **2017**, *233*, 457−466.
(38) Balamurugan, S.; Obubuafo, A.; Soper, S. A.; Spivak, D. A. A Surface immobilization methods for aptamer diagnostic applications. *Anal. Bioanal. Chem.* **2008**, *390*, 1009−1021.
(39) Love, J. C.; Estroff, L. A.; Kriebel, J. K.; Nuzzo, R. G.; Whitesides, G. M. Self-Assembled Monolayers of Thiolates on Metals as a Form of Nanotechnology. *Chem. Rev.* **2005**, *105*, 1103−1170.

https://dx.doi.org/10.1021/acsabm.0c00110
ACS Appl. Bio Mater. XXXX, XXX, XXX−XXX

(40) Johnson, P. B.; Christy, R. W. Optical-Constants Of Noble-Metals. *Phys. Rev. B: Condens. Matter Mater. Phys.* **1972**, *6*, 4370−4379.
(41) Hao, R.; Wang, D.; Zhang, X. e.; Zuo, G.; Wei, H.; Yang, R.; Zhang, Z.; Cheng, Z.; Guo, Y.; Cui, Z.; Zhou, Y. Rapid detection of Bacillus anthracis using monoclonal antibody functionalized QCM sensor. *Biosens. Bioelectron.* **2009**, *24*, 1330−1335.
(42) Unser, S.; Bruzas, I.; He, J.; Sagle, L. Localized Surface Plasmon Resonance Biosensing: Current Challenges and Approaches. *Sensors* **2015**, *15*, 15684−15716.
(43) Pandey, A. K.; Yudhishthir, P.; Rajput, S.; Sharma, R. Immobilized aptamer on gold electrode senses trace amount of aflatoxin M1. *Appl. Nanosci.* **2017**, *7*, 893−903.
(44) Tjong, V.; Tang, L.; Zauscher, S.; Chilkoti, A. Smart DNA interfaces. *Chem. Soc. Rev.* **2014**, *43*, 1612−1626.
(45) Elhadj, S.; Singh, G.; Saraf, R. F. Optical properties of an immobilized DNA monolayer from 255 to 700 nm. *Langmuir* **2004**, *20*, 5539−5543.
(46) Šiurkus, J.; Neubauer, P. Reducing conditions are the key for efficient production of active ribonuclease inhibitor in Escherichia coli. *Microb. Cell Factories* **2011**, *10*, 31.
(47) Dinges, M. M.; Orwin, P. M.; Schlievert, P. M. Exotoxins of Staphylococcus aureus. *Clin. Microbiol. Rev.* **2000**, *13*, 16−34.
(48) Staphylococcus aureus Toxin Formation in Hydrated Batter Mixes (A Biological Hazard). *Fish and Fishery Products Hazards & Controls Guide*, 2nd ed.; FDA, 1998; pp 183−188, Chapter 15.
(49) Dai, J.; Wu, S.; Huang, J.; Wu, Q.; Zhang, F.; Zhang, J. Prevalence and Characterization of Staphylococcus aureus Isolated From Pasteurized Milk in China. *Front. Microbiol.* **2019**, *10*, 641.
(50) *Compliance Policy Guide Sec. 527.300 Dairy Products—Microbial Contaminants and Alkaline Phosphatase Activity*; FDA, 2010; pp 1−10.
(51) Tyagi, A.; Saravanan, V.; Karunasagar, I.; Karunasagar, I. Detection of Vibrio parahaemolyticus in tropical shellfish by SYBR green real-time PCR and evaluation of three enrichment media. *Int. J. Food Microbiol.* **2009**, *129*, 124−130.
(52) Haynes, C. L.; Van Duyne, R. P. Nanosphere lithography: A versatile nanofabrication tool for studies of size-dependent nanoparticle optics. *J. Phys. Chem. B* **2001**, *105*, 5599−5611.
(53) Miller, M. M.; Lazarides, A. A. Sensitivity of Metal Nanoparticle Surface Plasmon Resonance to the Dielectric Environment. *J. Phys. Chem. B* **2005**, *109*, 21556−21565.

https://dx.doi.org/10.1021/acsabm.0c00110
ACS Appl. Bio Mater. XXXX, XXX, XXX−XXX